Dieses Dokument ist eine Zweitveröffentlichung (Postprint) /

This is a self-archiving document (accepted version):

Martin Weiher, Melanie Herzig, Ronald Tetzlaff, Alon Ascoli, Thomas Mikolajick, Stefan Slesazeck

Pattern Formation With Locally Active S-Type NbOx Memristors

Erstveröffentlichung in / First published in:

IEEE Transactions on Circuits and Systems : a publication of the IEEE Circuits and Systems Society. 1, Regular Papers. 2019, 66(7), S. 2627-2638 {Zugriff am: 18.08.2021}. IEEE. ISSN 1558-0806.

DOI: https://doi.org/10.1109/TCSI.2019.2894218

Diese Version ist verfügbar / This version is available on:

https://nbn-resolving.org/urn:nbn:de:bsz:14-qucosa2-767760

SLUB Wir führen Wissen.

TECHNISCHE UNIVERSITÄT DRESDEN

QUCOSA Quality Content of Saxony

Final edited form was published in "IEEE Transactions on Circuits and Systems : a publication of the IEEE Circuits and Systems Society. 1, Regular Papers. 2019, 66(7), S. 2627-2638. ISSN 1558-0806.
https://doi.org/10.1109/TCSI.2019.2894218

Pattern Formation With Locally Active S-Type NbO_x Memristors

Martin Weiher, Melanie Herzig, Ronald Tetzlaff, *Senior Member, IEEE*, Alon Ascoli, Thomas Mikolajick, *Senior Member, IEEE*, and Stefan Slesazeck

***Abstract*— The main focus of this paper is the evolution of complex behavior in a system of coupled nonlinear memristor circuits depending on the applied coupling conditions. Thereby, the parameter space for the local activity and the edge-of-chaos domain will be determined to enable the emergence of the pattern formation in locally coupled cells according to Chua's principle. Each cell includes a Niobium oxide-based memristor, which may feature a locally active behavior once it is suitably biased on the negative differential resistance region of its DC current-voltage characteristic. It will be shown that there exists a domain of parameters under which each uncoupled cell may become locally active around a stable bias state. More specifically, under these conditions, the coupled cells are on the edge-of-chaos, and can support the static and dynamic pattern formation. The emergence of such complex spatio-temporal behavior in homogeneous structures is a prerequisite for information processing. The theoretical results are confirmed by measurements as well as by the numerical simulations of the accurate device and circuit models.**

***Index Terms*— Local activity, edge-of-chaos, memristor, nonlinear dynamics, pattern formation.**

I. Introduction

PROCESSORS in computing structures are usually based on a von-Neumann architecture, where the memory system and the processing unit are separated. While, in recent years, a significant enhancement in the processor speed has been achieved, research and development on memory systems have been focused on density increase only. Since the operating speed in traditional computing machines is limited by the data transfer rate along the bus between memory and central processing unit, any possible enhancement in processor functionalities is impeded by the limited bandwidth of this channel, the so-called von-Neumann bottleneck. For the realization of communicating sensor-processor systems in cyber physical systems, new more effective processing architectures have to be developed in order to combine data storage and processing units more efficiently. Furthermore, the still ongoing shrinking of transistor dimensions, as predicted by Moore's law, can be expected to come to an end very soon. Consequently, traditional circuits should be replaced by those exploiting the dynamic behavior of appropriate time- and power-efficient nano-electronics devices in future information processing systems.

Since in 2007 Stanley Williams and his team at Hewlett Packard Labs made a first conscious connection between the electrical characterizations of the nano-electronic device fabricated within their premises and the fingerprints of memristors (see [1]) outlined in the 1971 seminal paper [2] of Leon Chua, various investigations have been demonstrating the huge potential of these devices in overcoming the limits of conventional CMOS technology. Especially, since memristors allow to carry out signal processing and data storage operations in the same physical nano-scale location, they pave the way toward the development of the so-called in-memory computing structures, which, in the form of memristor array architectures, have already shown an enormous potential in overcoming the von-Neumann bottleneck, e.g. enabling the implementation of sensor-processor systems for the real-time analysis of multidimensional signals. Recently, fabricated crossbar structures have been considered to perform correlation detection, and, especially, to carry out certain linear algebra calculations in a single operation, paving the way toward the implementation of in-memory computing or bio-inspired signal processing strategies. Typically, bio-inspired computing is based on networks consisting of identical cells interacting within a certain range with neighboring cells. In this context, realizations of programmable computing structures, based on Cellular Neural Networks (CNN), which are characterized by local couplings among nonlinear dynamical systems of relatively-low complexity, called cells, have already demonstrated a significantly-high performance, especially in computer vision applications. In principle, complex problems can be solved by exploiting the dynamic behavior of locally-interacting cells, as shown in various application fields, including the real-time control of laser welding processes [3].

Depending on the network topology and on the coupling structure, different network properties are addressable. For instance, a network consisting of oscillatory cells can be

Manuscript received July 23, 2018; revised November 24, 2018 and December 18, 2018; accepted January 4, 2019. Date of publication February 14, 2019; date of current version June 18, 2019. This work was supported by the Deutsche Forschungsgemeinschaft (DFG, German Research Foundation), under Project 273537230, respectively, under Grant MI 1247/12-1. This paper was recommended by Associate Editor A. James. *(Corresponding author: Martin Weiher.)*

M. Weiher, A. Ascoli, and R. Tetzlaff are with the Faculty of Electrical and Computer Engineering, Institute of Circuits and Systems, Technische Universität Dresden, D-01062 Dresden, Germany (e-mail: martin.weiher@tu-dresden.de).

M. Herzig and S. Slesazeck are with the Nanoelectronic Materials Laboratory gGmbH, D-01187 Dresden, Germany.

T. Mikolajick is with the Nanoelectronic Materials Laboratory gGmbH, D-01187 Dresden, Germany, and also with the Faculty of Electrical and Computer Engineering, Institute of Semiconductors and Microsystems, Technische Universität Dresden, D-01062 Dresden, Germany.

Color versions of one or more of the figures in this paper are available online at http://ieeexplore.ieee.org.

Provided by Sächsische Landesbibliothek - Staats- und Universitätsbibliothek Dresden

Final edited form was published in "IEEE Transactions on Circuits and Systems : a publication of the IEEE Circuits and Systems Society. 1, Regular Papers. 2019, 66(7), S. 2627-2638. ISSN 1558-0806.
https://doi.org/10.1109/TCSI.2019.2894218

used for brain-inspired spike-based computing. Hereby, the so-called neuristor, consisting of two simple resistively-coupled memristor oscillatory circuits, has been considered as electronic emulator of the Hodgkin-Huxley axon, see [4]. In general, the emergence of complex behaviors, characterized by non-homogeneous solutions (e.g. pattern formation), can be observed in various homogeneous networks, i.e. structures of identical elements with space-invariant couplings. Taking spatially-discretized reaction-diffusion CNN (RD-CNN) (see [5] and [6]) as reference for the theoretical analysis, Chua has proved that local activity is the origin of complexity. For example, locally-active RD-CNN cells can exhibit limit cycles or chaos. Local activity follows when cells can amplify the power resulting from current and voltage of the cell state equations linearized at an equilibrium point. For instance the transistor as basic device in state-of-the-art signal processing units can be classified as a locally-active device [5]. Most importantly for the work presented in this manuscript, other locally-active devices are those memristor realizations, e.g. the NbO_x, TaO_x, TiO_x and VO_2 memristors, shown in [7]–[10], based on threshold switching effects, exhibiting a negative differential resistance (NDR) region in their DC current-voltage characteristic.

In this paper we propose a novel Memristor-CNN (M-CNN), composed of cells interacting locally through RC-bridge coupling circuits and including NbO_x devices within their topology. By applying the local activity theorem of Leon Chua, we analytically derive appropriate coupling parameters for the emergence of static and dynamic pattern formation in the resulting M-CNN. Thereby, a map of the RC coupling parameters has been derived, and the region of local activity, and, particularly, of the edge-of-chaos, necessary for the emergence of complex behavior within the nonlinear dynamic array, was identified. The spatio-temporal phenomena arising at steady state in the cellular network when the cells operate in the sharp edge-of-chaos are thoroughly discussed in this paper, since, in the future, they shall be exploited to implement new forms of computing paradigms.

Unlike the study presented in [9], this work performs an in-depth theoretical analysis of system properties. Theoretical results are validated through both numerical simulations and experimental measurements. Particularly, regarding the numerical simulations, a robust NbO_x device model was developed, taking into account that the threshold switching behavior of our memristor nano-device originates from a Frenkel-Poole-like conduction mechanism favored by thermal feedback effects. Remarkably, some parasitic effects, observed over the course of the experimental measurements, have been considered in the device model. As compared to investigations reported in past works, and dealing with the synchronization among coupled oscillators [11], i.e. between cells which would oscillate already on their own, the focus is here on the birth of certain oscillations in nonlinear dynamical arrays resulting from appropriate couplings among otherwise sleeping cells.

This paper is structured as follows. The principle framework necessary for applying Chua's theory of local activity is described in section II. Thereby, the structure treated here will be adapted to this framework. The modeling of the memristor cell is described in section III. Particularly, the fitting parameters of the real memristor model will be extracted for two distinct devices in order to capture accurately their behaviors. Section IV applies the principle of local activity to the cells considered in this contribution. Regions of the R-C coupling parameter space, characterizing different dynamic properties, including the support of static and dynamic patterns, of the memristor network under study, will be determined. In section V theoretical results shall be compared to experimental measurements and numerical simulations on a two cell network for different coupling parameters. Additionally, the pattern formation in a memristor cell array shall be illustrated and discussed for two interesting coupling scenarios. Finally, conclusions, including future aspects of this research project, and a discussion of some of the challenging problems we shall be facing towards the achievement of our goals, are drafted in section VI.

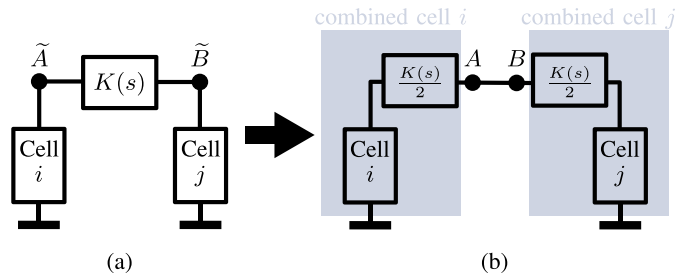

Fig. 1. Allocation of the coupling to the cells. (a) Two cells with linear dynamic coupling $K(s)$. (b) Two combined cells with allocated coupling impedance $K(s)/2$.

II. Main Idea

The aim of this paper is the investigation of complex behavior in locally coupled memristive cells based on Chua's principle of local activity [6] which has been derived for dissipative couplings. Thus, in order to fulfill the prerequisites necessary to apply Chua's principle of local activity, the cells have to be coupled through resistors. However, within the investigated network an additional capacitive element needs to be included to achieve a larger variety in the resulting behaviors. The problem can be solved by an allocation of part of this coupling circuit to each of the cells in the network, as shown in the simple example of Fig. 1. The coupling is established by a linear dynamic system placed between the ports $\widetilde{A}$ and $\widetilde{B}$, which is illustrated by the impedance $K(s)$ in the Laplace domain, see Fig. 1(a). To be able to apply the theory of local activity, we split this coupling impedance in two equal parts, which are allocated one to the left cell and the other to the right cell. Thus, we obtain a new combined cell, which consists of the original cell and a half of the coupling impedance, see Fig. 1(b). Between the separated coupling impedances, each equal to $K(s)/2$, there are the new coupling ports A and B. Between these ports there is a direct connection, i.e. a resistive coupling with a resistance of $0\,\Omega$, allowing the application of the principle of local activity.

For our resistor-capacitor bridge with the capacitor $\widetilde{C}$ and the resistor $\widetilde{R}$, $K(s)$ is given by

$$K(s) = \frac{\widetilde{R}}{1 + s\widetilde{C}\widetilde{R}}. \tag{1}$$

Provided by Sächsische Landesbibliothek - Staats- und Universitätsbibliothek Dresden

Final edited form was published in "IEEE Transactions on Circuits and Systems : a publication of the IEEE Circuits and Systems Society. 1, Regular Papers. 2019, 66(7), S. 2627-2638. ISSN 1558-0806.
https://doi.org/10.1109/TCSI.2019.2894218

Consequently the separated coupling is also an resistor-capacitor bridge with the capacitor C and the resistor R obtainable as follows

$$\frac{K(s)}{2} = \frac{R}{1+sCR} \quad \text{with: } C = 2\widetilde{C} \text{ and } R = \frac{\widetilde{R}}{2}. \tag{2}$$

III. Modeling

In this section, the cell model will be introduced. An accurate model for the real memristor device will be derived by combining the physical model of an NbO_x memristor with parasitic contributions, which are unavoidable in practice. Finally, the equivalent circuit of the complete cell will be introduced and discussed.

A. Threshold Switching Model of Idealized NbO_x Memristor

It has been shown in [12]–[19] that the switching behavior of NbO_x based memristive devices can be explained via a Frenkel-Poole like conduction mechanism linked with thermal feedback effects. Based on the laws of physics, a compact mathematical model for an idealized NbO_x memristor M was developed. The current-voltage relation is cast as

$$v_M = M(T, v_M)\, i_M, \tag{3}$$

where v_M denotes the voltage drop across and i_M the current through the memristor. T is the temperature of the memristor filament, and is chosen as memory state. The memristor model can be described by a differential algebraic equation (DAE) set, where the device current and voltage are linked by the memristance, expressed by

$$M(T, v_M) = R_0\, e^{\frac{\alpha_0 + \alpha_1\sqrt{v_M} + \alpha_2 v_M}{T}} \tag{4}$$

through equation (3), while a thermal differential equation governs the time evolution of the memristor state according to the power balance law

$$C_{th}\dot{T} = v_M i_M + \Gamma_{th}(T_{amb} - T), \tag{5}$$

where R_0, α_0, α_1, and α_2 are parameters of the memristance, C_{th} and Γ_{th} indicate the thermal capacitance and conductance, respectively, whereas T_{amb} stands for the ambient temperature.

In principle, the DAE set (3)-(5) is a mathematical combination of the physical models describing the memristances $M^\star$ and $M^{\star\star}$ published in [16] and [17]. The memristance published in [16] can be calculated as

$$M^\star(T, v_M) = R_0\, e^{\frac{\alpha_0^\star + \alpha_1^\star\sqrt{v_M}}{T}} \tag{6}$$

with

$$\alpha_0^\star = \frac{E_a}{k}, \tag{7a}$$

$$\alpha_1^\star = -\sqrt{\frac{q^3}{k^2\pi\varepsilon_0\varepsilon_r t_{ox}}} \tag{7b}$$

and

$$R_0 = \frac{4t_{ox}}{N_C\mu q\pi {d_{fil}}^2}. \tag{8}$$

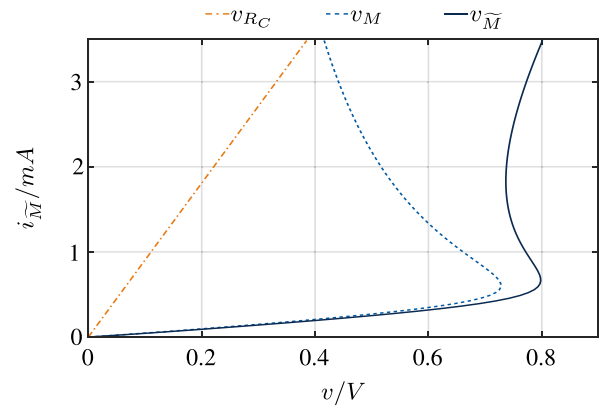

Fig. 2. Quasi-static current-voltage characteristic of the memristor $\widetilde{M}_1$ with model parameters fitted as shown in Table I. Illustrated is the voltage $v_{\widetilde{M}}$ across the real device, consisting of the combination between the voltage v_M across the idealized NbO_x memristor and the voltage v_{R_C} across the contact resistor R_C.

Here N_C denotes the density of states in the conduction band, μ the electron mobility, d_{fil} the diameter of the filament, E_a the activation energy, q the elementary charge, t_{ox} the effective oxide thickness, ε_0 and ε_r the vacuum and the relative permittivity, while k signifies the Boltzmann constant. In this model, the lowering of the activation energy is proportional to the square root of the voltage drop across the memristor. The model in [17] considers also the barrier lowering effect induced by the large donor state concentration N_D, which needs to be taken into account especially in the high current regime, where our nano-device experiences non-volatile resistive switching. In [17] the memristance assumes then the following form:

$$M^{\star\star}(T, v_M) = R_0\, e^{\frac{\alpha_0^{\star\star} + \alpha_2^{\star\star} v_M}{T}} \tag{9}$$

with

$$\alpha_0^{\star\star} = \frac{E_a}{k} - \frac{q^2 {N_D}^{1/3}}{4k\pi\varepsilon_0\varepsilon_r} \tag{10a}$$

and

$$\alpha_2^{\star\star} = -\frac{q\lambda}{kt_{ox}}, \tag{10b}$$

where λ is a fitting parameter describing the de-centering of the maximum of the potential barrier between the donor states. Hence (4) physically characterizes the overall device memristance as a superposition between a contribution described by (6), accounting for threshold switching dynamics and a contribution described by (9), capturing the emergence of non-volatile resistive switching in the high current regime.

B. Comprehensive Model of Real NbO_x Memristor Including Parasitics

In case of a real device $\widetilde{M}$, certain parasitics have to be taken into account, especially the contact resistance R_C. Due to the increasing voltage drop over R_C for increasing currents, the externally accessible voltage range of the NDR region in the DC current-voltage characteristic is reduced. However, a wide NDR region is of utmost importance for the generation of robust oscillations. In Fig. 2 the effect of R_C on memristor

Provided by Sächsische Landesbibliothek - Staats- und Universitätsbibliothek Dresden

Final edited form was published in "IEEE Transactions on Circuits and Systems : a publication of the IEEE Circuits and Systems Society. 1, Regular Papers. 2019, 66(7), S. 2627-2638. ISSN 1558-0806.
https://doi.org/10.1109/TCSI.2019.2894218

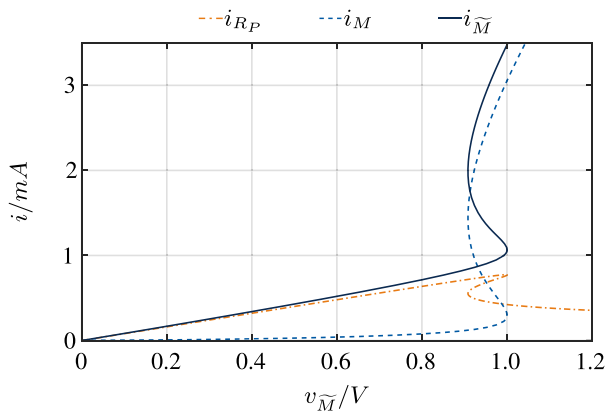

Fig. 3. Quasi-static current-voltage characteristic of the memristor $\widetilde{M}_2$ with model parameters fitted as shown in Table I. Illustrated is the current $i_{\widetilde{M}}$ through the real device, which consists of the combination between the current i_M through the idealized NbO$_x$ memristor and the current i_{R_P} through the parasitic resistor R_P.

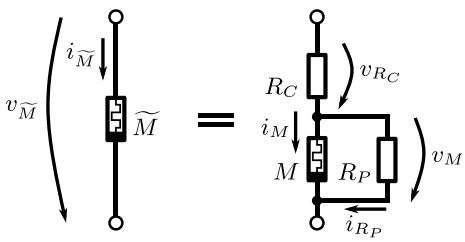

Fig. 4. Structure of a real NbO$_x$ device $\widetilde{M}$.

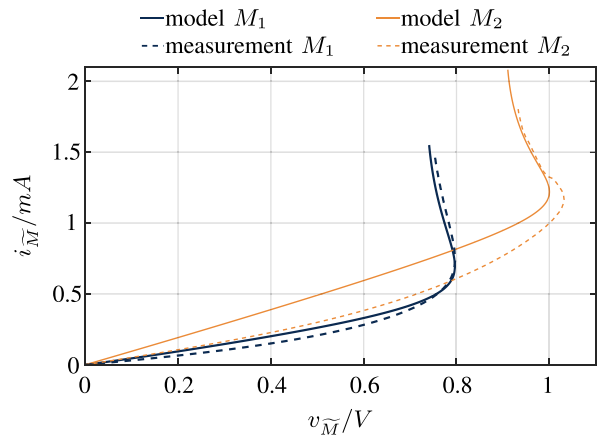

Fig. 5. Model validation for two devices $\widetilde{M}_1$ and $\widetilde{M}_2$ via quasi-static measurements.

TABLE I
MODEL PARAMETERS USED TO FIT THE MEASURED CURVES IN FIG. 5

	$\widetilde{M}_1$	$\widetilde{M}_2$	
R_0	0.80	1.27	Ω
α_0	2923	3146	K
α_1	-628.0	-470.7	$K/\sqrt{V}$
α_2	402.1	-26.7	K/V
C_{th}	$1.324 \cdot 10^{-13}$	$7.661 \cdot 10^{-15}$	J/K
Γ_{th}	$5.953 \cdot 10^{-6}$	$4.790 \cdot 10^{-6}$	W/K
T_{amb}	298	298	K
R_P	2930	1082	Ω
R_C	110	156	Ω

voltages is illustrated. The quasi-static current-voltage characteristic corresponding to the real device $\widetilde{M}$ (black line) exhibits a narrower NDR region as compared to the idealized memristor M (blue line) under the effect of the contact resistance R_C (orange line) (see Fig. 4). Another parasitic effect results from a parallel resistance R_P, which models the leakage current through the device. Fig. 3 illustrates the currents $i_{\widetilde{M}}$, i_M, and i_{R_P}, respectively flowing through the real memristor $\widetilde{M}$ (black curve), the idealized device M (blue curve), and the parasitic resistor R_P (orange curve) (see Fig. 4). In the low current regime ($\leq 0.5\,mA$) i_{R_P} dominates the total current flowing through the real memristor device $\widetilde{M}$, while in the high current regime ($\geq 1.5\,mA$), i_M provides the most significant contribution to $i_{\widetilde{M}}$.

Thus, the model of a real memristor device $\widetilde{M}$ comprises of the idealized NbO$_x$ memristor M and these two parasitic resistors, as shown in Fig. 4. In order to account for the parasitics, the voltage $v_{\widetilde{M}}$ and current $i_{\widetilde{M}}$ of the real device can be expressed via the voltage v_M and current i_M of the idealized memristor as follows

$$v_{\widetilde{M}} = \left(1 + \frac{R_C}{R_P}\right) v_M + R_C i_M, \tag{11a}$$

$$i_{\widetilde{M}} = \frac{1}{R_P} v_M + i_M. \tag{11b}$$

In Fig. 5 the solutions computed from the real device model are compared to measurement results. The model parameters for two distinct NbO$_x$ memristor devices, obtained by means of an optimization procedure applied to the respective measured quasi-static current-voltage characteristic, are summarized in Table I. To perform the measurement of the characteristics of Fig. 5 the memristor $\widetilde{M}_1$ ($\widetilde{M}_2$) with series resistance $R_S = 5530\,\Omega$ ($R_S = 5545\,\Omega$) was driven by a sufficiently slow purely-positive voltage ramp V_S swept from $0\,V$ to $9\,V$ ($11\,V$). The temperature characteristics extracted from the models of the two devices are illustrated in Fig. 6. Finally, it can be observed that for each of the two devices the NDR region is accurately captured by the proposed model, which is necessary, because the main dynamical properties of the networks considered here critically require each cell memristor to be biased in this region. Most differences between model predictions and measurements arise under low currents. We conjecture that these deviations may be attributed to nonlinearities in the behavior of the parallel parasitic resistor, which in the model is assumed to be of constant resistance R_P, but, most probably, is a voltage- or temperature-dependent resistor.

C. Combined Memristor Cell

The combined memristor cell, shown in Fig. 7, consists of a real NbO$_x$ memristor $\widetilde{M}$, its biasing circuit, i.e. the series between a DC voltage source V_S and a linear resistor of resistance R_S, and a RC-bridge. Its output port is called A.

Provided by Sächsische Landesbibliothek - Staats- und Universitätsbibliothek Dresden

Final edited form was published in "IEEE Transactions on Circuits and Systems : a publication of the IEEE Circuits and Systems Society. 1, Regular Papers. 2019, 66(7), S. 2627-2638. ISSN 1558-0806.
https://doi.org/10.1109/TCSI.2019.2894218

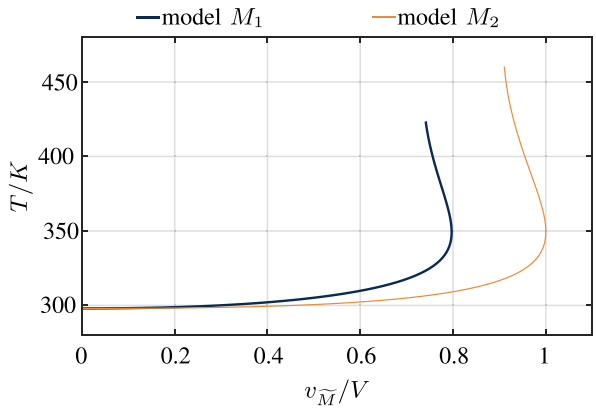

Fig. 6. Temperature characteristics extracted from the models of $\widetilde{M}_1$ and $\widetilde{M}_2$.

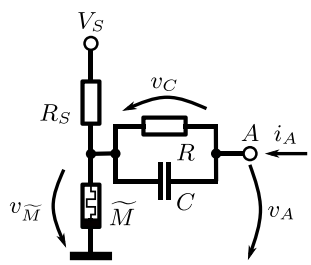

Fig. 7. Combined memristor cell with RC-bridge and coupling port A.

The coupling of two combined cells of this kind is realized via a simple wire of zero resistance connecting the respecting output ports. Using the real memristor model introduced in section III-B, the combined cell can be described by the DAE set

$$\mathbf{E}\dot{\mathbf{x}} = \mathbf{f}(\mathbf{x}, i_A) \tag{12}$$

where the state vector is defined as

$$\mathbf{x} = \begin{pmatrix} x_1 & x_2 & x_3 & x_4 \end{pmatrix}^\top = \begin{pmatrix} T & v_C & v_M & i_M \end{pmatrix}^\top, \tag{13}$$

$\mathbf{E}$ is the singular diagonal matrix expressed by

$$\mathbf{E} = \begin{pmatrix} C_{th} & 0 & 0 & 0 \\ 0 & RC & 0 & 0 \\ 0 & 0 & 0 & 0 \\ 0 & 0 & 0 & 0 \end{pmatrix}, \tag{14}$$

while the vector field $\mathbf{f}(\mathbf{x}, i_A)$ takes the following form

$$\mathbf{f}(\mathbf{x}, i_A) = \begin{pmatrix} x_3 \; x_4 - \Gamma_{th}(x_1 - T_{amb}) \\ -x_2 + R i_A \\ x_3 - M(x_1, x_3) x_4 \\ R_p V_S - R_\Sigma x_3 - R_\Pi R_P x_4 + R_S R_P i_A \end{pmatrix}, \tag{15}$$

with

$$R_\Sigma = R_P + R_S + R_C, \tag{16a}$$
$$R_\Pi = R_S + R_C. \tag{16b}$$

Note that v_M (v_C) denotes the voltage drop across the memristor (capacitor) terminals, while i_M stands for the current flowing through the memristor. Furthermore, the current entering port A is called i_A. The output voltage v_A at port A is given by

$$v_A = \begin{pmatrix} 0 & 1 & 1 + \dfrac{R_C}{R_P} & R_C \end{pmatrix} \mathbf{x} = \mathbf{C}\mathbf{x}. \tag{17}$$

IV. Local Activity and the Edge-of-Chaos

This section studies the dynamical phenomena emerging in the two-cell network presented in section III-C. The influence of the coupling capacitor on the oscillation frequency of a two-memristive cell network is discussed in [9]. As a novelty, the aim of our work is to understand how uncoupled cells with stationary steady-state solutions have to be coupled to become alive, that is to admit a distinct set of stationary solutions (the so called static patterns) or oscillations (known as dynamic patterns) at steady state. The network behavior can be changed by tuning the operating point of each memristor via V_S and R_S or by tuning the coupling parameters R and C. This work will focus on the influence of the coupling parameters on the dynamic properties of the network. The memristor is always biased on the NDR region of its DC current-voltage characteristic by keeping V_S and R_S unaltered. In the Appendix some of the effects arising from a shift in the memristor operating point, caused by a change in V_S, are illustrated. The well-known principle of local activity proposed by Chua provides the basis for the investigations discussed in the following. Chua has shown that local activity is the origin of complexity. It is the fundamental principle enabling the emergence of inhomogeneous solutions (i.e. static or dynamic patterns) in networks of identical structures, which would otherwise admit only trivial stationary homogeneous solutions. This implies that an array of identical cells coupled by means of linear resistors is capable to support spatio-temporal patterns in the voltage or current domain, if and only if these cells are locally active. With reference to the network proposed in section III-C, the combined memristor cells may become alive upon coupling provided they operate in locally active mode.

A. Input Impedance of the Linearized Cell

Necessary criteria for the local activity of RD-CNNs, composed of identical resistively-coupled cells, were derived in [6]. In order to apply the theory of local activity, the input impedance Z at port A of the system, linearized around the steady state $\bar{\mathbf{x}}$ without coupling (i.e. for $i_A = \bar{i}_A = 0$), has to be determined. This may be achieved by setting equation (12) to 0 under zero port current, i.e.

$$\mathbf{f}(\bar{\mathbf{x}}, 0) = \mathbf{0}. \tag{18}$$

Recasting the current at port A, the voltage at port A, and the state as the sum between a steady-state component and a small perturbation around it, according to

$$v_A = \bar{v}_A + \tilde{v}_A, \tag{19a}$$
$$i_A = \bar{i}_A + \tilde{i}_A = \tilde{i}_A, \tag{19b}$$
$$\mathbf{x} = \bar{\mathbf{x}} + \tilde{\mathbf{x}}, \tag{19c}$$

Provided by Sächsische Landesbibliothek - Staats- und Universitätsbibliothek Dresden

Final edited form was published in "IEEE Transactions on Circuits and Systems : a publication of the IEEE Circuits and Systems Society. 1, Regular Papers. 2019, 66(7), S. 2627-2638. ISSN 1558-0806.
https://doi.org/10.1109/TCSI.2019.2894218

TABLE II
LOCAL INPUT IMPEDANCE $Z_i(s)$ OF THE COMBINED MEMRISTOR CELL OF FIG. 7 WITH MEMRISTOR DEVICE $\widetilde{M}_i$ $(i \in \{1,2\})$ FROM TABLE I

	V_S	R_S	R	C
$Z_1(s)$	$9\,V$	$5530\,\Omega$	$1.0\,M\Omega$	$720\,pF$
$Z_2(s)$	$11\,V$	$5545\,\Omega$	$1.0\,M\Omega$	$720\,pF$

and then applying a Taylor series expansion to (12) and (17) around the uncoupled steady state, the linearized system assumes the following form

$$\mathbf{E}\dot{\tilde{\mathbf{x}}} = \mathbf{A}\tilde{\mathbf{x}} + \mathbf{B}\tilde{i}_A \tag{20a}$$

$$\tilde{v}_A = \mathbf{C}\tilde{\mathbf{x}} + D\tilde{i}_A \tag{20b}$$

where

$$\mathbf{A} = \left.\frac{\partial \mathbf{f}}{\partial \mathbf{x}}\right|_{\mathbf{x}=\bar{\mathbf{x}}, i_A=0}, \tag{21a}$$

$$\mathbf{B} = \left.\frac{\partial \mathbf{f}}{\partial i_A}\right|_{\mathbf{x}=\bar{\mathbf{x}}, i_A=0}, \tag{21b}$$

$$\mathbf{C} = \begin{pmatrix} 0 & 1 & 1 + \dfrac{R_C}{R_P} & R_C \end{pmatrix}, \tag{21c}$$

$$D = 0. \tag{21d}$$

Thus, the cell local input impedance in the Laplace domain is found to be expressed by

$$Z(s) = \frac{\tilde{V}_A(s)}{\tilde{I}_A(s)} = \mathbf{C}(s\mathbf{E} - \mathbf{A})^{-1}\mathbf{B} \tag{22}$$

where s is the Laplace variable, while $\tilde{V}_A(s)$ and $\tilde{I}_A(s)$ are the Laplace transforms of $\tilde{v}_A(t)$ and $\tilde{i}_A(t)$, respectively. The input impedances of two memristor cells, respectively using the real memristor devices $\widetilde{M}_1$ and $\widetilde{M}_2$ from section III-B and the parameters listed in the first and second rows of Table II, are given by

$$Z_1(s) = 450.9\frac{s^2 - 3.416 \cdot 10^6 s + 2.987 \cdot 10^{14}}{(s + 9.696 \cdot 10^7)(s + 1389)} \tag{23a}$$

and

$$Z_2(s) = 391.1\frac{s^2 - 6.515 \cdot 10^7 s + 3.264 \cdot 10^{15}}{(s + 9.192 \cdot 10^8)(s + 1389)}. \tag{23b}$$

B. Conditions for Local Activity and Edge-of-Chaos

The following conditions were derived in [6] by Chua on the basis of the RD-CNN modeling equations. A network of identical resistively-coupled cells is locally active if at least one of the following conditions on its local input impedance is fulfilled:

(i) $Z(s)$ has a pole in $\Re\{s\} > 0$.
(ii) $Z(s)$ has a multiple pole on the imaginary axis.
(iii) $Z(s)$ has a simple pole $s = i\omega_p$ on the imaginary axis and $\lim_{s \to i\omega_p}(s - i\omega_p)Z(s)$ is either a negative-real number, or a complex number.
(iv) There is at least one $\omega \in \mathbb{R}$ so that $\Re\{Z(i\omega)\} < 0$ holds true.

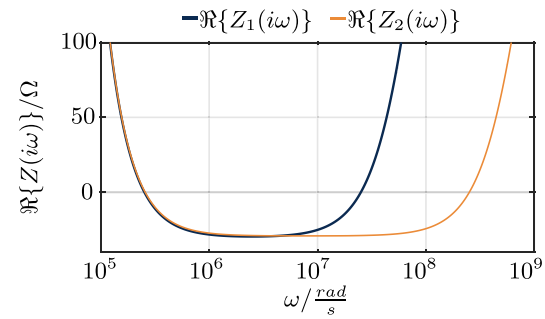

Fig. 8. Test for condition (iv) for the two combined cells of the network.

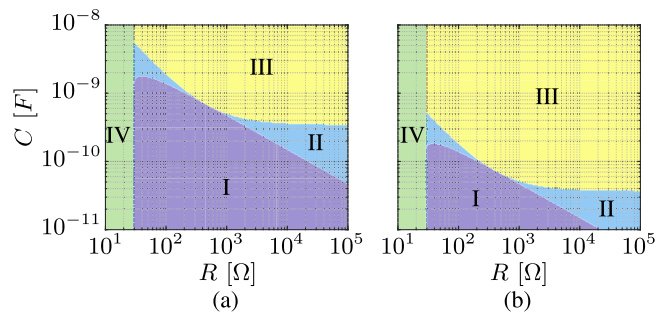

Fig. 9. RC coupling parameter plane for (a) $Z_1(s)$ and (b) $Z_2(s)$. The violet part I contains the parameter combinations where $Z(s)$ is locally passive. The rest of the parameter plane represents the region where the system is stable and locally-active. In the light blue domain II the system is on the edge-of-chaos. The sharp-edge-of-chaos region, where the cell local input impedance admits two positive zeros (one positive real zero) in the right half of the complex plane is the yellow domain III (green domain IV).

Here $\Re\{s\}$ describes the real part of s, while i denotes the imaginary unit. While conditions (i)-(iii) are associated to an unstable locally-active system, condition (iv) characterizes a stable locally-active system. A system, which is both stable and locally active, i.e. for which only (iv) in the aforegiven set of conditions applies, is said to be on the edge of chaos. Edge-of-chaos is that particular sub-domain of the locally-active domain, where complexity may truly emerge in the system. From equations (23a) and (23b) it may be easily inferred that for each of the cell local input impedances $Z_1(s)$ and $Z_2(s)$ the two poles lie in left half of the complex plane. Thus, conditions (i)-(iii) are not met for either of the two cells, which are thus stable. In order to check whether the cells are locally active, condition (iv) has to be inspected. Hence, for each of the two cell local input impedances, we need to determine whether there exists at least one angular frequency ω such that $\Re\{Z(i\omega)\} < 0$. From the graphs in Fig. 8, it can be inferred that indeed for each of the two cells under consideration there is a range of ω, where $\Re\{Z(i\omega)\} < 0$. Thus, these two cells are stable and locally active, i.e. they are on the edge-of-chaos.

C. Parameter Set for Local Activity and (Sharp) Edge-of-Chaos

Testing the local activity conditions (i)-(iv) for each of the two network cells under all possible combinations of R and C within certain prescribed ranges leads to a partition of the coupling parameter space into two main subspaces, as shown in Fig. 9. The violet subspace I contains (R, C) pairs referring

Provided by Sächsische Landesbibliothek - Staats- und Universitätsbibliothek Dresden

Final edited form was published in "IEEE Transactions on Circuits and Systems : a publication of the IEEE Circuits and Systems Society. 1, Regular Papers. 2019, 66(7), S. 2627-2638. ISSN 1558-0806.
https://doi.org/10.1109/TCSI.2019.2894218

to a locally-passive cell. The union of the light blue II, yellow III, and green IV domains is the set of locally-active parameters. Here, for each of the two cells, the edge-of-chaos sub-domain coincides with the locally-active domain, because only (iv) within the set of conditions (i)-(iv) is fulfilled for each (R, C) pair in the locally-active parameter set. Provided it is stable and locally-active, a system can be destabilized only for a subset of the coupling parameter combinations within the edge-of-chaos domain. As Chua demonstrated in [6], diffusive i.e. resistive couplings among cells can destabilize a network of identical cells if and only if the cells are on the sharp-edge-of-chaos, which is a proper subset of the edge-of-chaos domain for which at least one zero $z \in \mathbb{C}$ of the cell local input impedance $Z(s)$ lies in the right half of the complex plane, i.e. $\Re\{s\} > 0$. In Fig. 9 one of the edge-of-chaos regions, i.e. light blue domain II, contains coupling parameters, which may not destabilize the system, since the resulting cell local input impedance has no zero with positive real part. On the other hand, the union of the yellow III and green IV subsets represents the sharp-edge-of-chaos domain. In the yellow domain III the cell local input impedance admits a pair of complex conjugate zeros with positive real part, enabling system destabilization leading to dynamic pattern formation at steady state. In the green domain IV one zero of the cell local input impedance is positive and real, triggering the destabilization of the system with the asymptotic emergence of static patterns.

V. Measurements and Simulation Results

A. Two Coupled Cells

In this section the validation of our theoretical results will be provided. The combined memristor cells of Table II will be coupled at port A, and the time behaviors of the voltages across the respective memristors will be investigated for different coupling parameters. With regard to the numerical simulations an implicit Runge-Kutta method, specifically the Radau-IIA 5th order method, was used in Matlab R2017b. Details of the manufacturing process of the memristor devices, each with a device area ranging between $0.4\,\mu m^2$ and $0.6\,\mu m^2$, electrically characterized for model development and then employed in the two-cell network implementation, are given in [17]. Measurements were carried out through a Keithley 4200 SCS and a Tektronix oscilloscope.

This section shall investigate the coupling between two slightly different combined cells, taking the effect of memristor device to memristor device variability into account. Although Chua's principle of local activity deals with the emergence of inhomogeneous solutions in homogeneous structures, in view of the expected scenarios in future hardware implementations, it is of interest to apply this theory to almost homogeneous structures with slightly different cells. In this way we shall predict the behavior of our network with two slightly different combined memristor cells, and we will validate our theoretical predictions with numerical simulation results, and, most importantly, experimental measurements. The behaviors of the two uncoupled cells are illustrated in Fig. 10(a). Each of the two uncoupled systems is in a

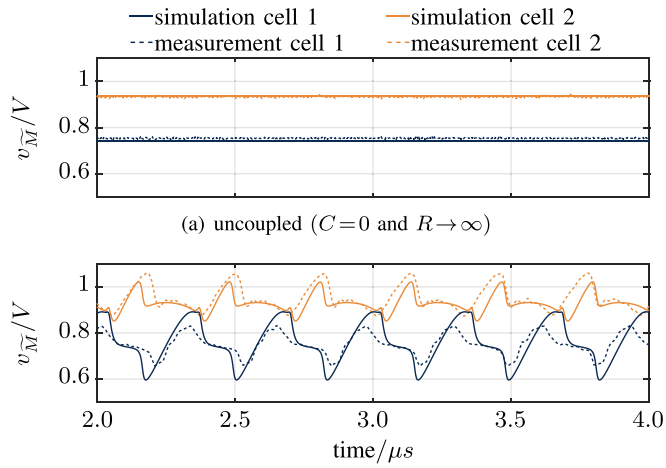

(a) uncoupled ($C = 0$ and $R \to \infty$)

(b) coupled ($C = 720\,pF$ and $R = 1\,M\Omega$)

Fig. 10. Voltages across the memristors of the two cell over time in the uncoupled case ((a) with $C = 0$ and $R \to \infty$) and in the uncoupled scenario ((b) with $C = 720\,pF$ and $R = 1\,M\Omega$). Numerical simulation results are depicted together with experimental measurements for comparison purposes.

stationary steady state. Measured data and numerical simulation results are in good agreement. In this uncoupled case each of the two combined cells does not include a RC-bridge. In other words the coupling parameters are here $C = 0$ and $R \to \infty$. Each cell contains a memristor biased on the NDR region by the voltage source V_S and its series resistance R_S (see Table II). However, each of the two cells is unable to wake up from the sleep mode on its own. The coupled case is presented in Fig. 10(b). From theory, the pair corresponding to $C = 720\,pF$ and $R = 1\,M\Omega$ is located in the sharp-edge-of-chaos yellow domain III of the coupling parameter space of each cell (see Figs. 9(a)-(b)). Clearly, the expected oscillatory solutions can be observed in the measurements and numerical simulation results depicted in Fig. 10(b), validating our theoretical results in unison. The small differences in amplitude and frequency between experiments and model predictions can be explained by the influence of noise in the real measurement setup and by slight deviations in the data fitting procedure. Another investigation was then carried out to prove the existence of the different regions in the coupling parameter plane (see Fig. 9). It is of special interest to understand what is the network behavior in case the coupling parameter pair associated to one cell sets it into one of the two sharp-edge-of-chaos sub-domains, while the choice of R and C for the other cell keeps it in the sleeping mode as in the uncoupled case. In Fig. 12 the steady-state behaviors of the two combined cells for four different choices of the common coupling parameter pair are presented. In Fig. 12(a) ((d)) the pair (R, C) is located in the dynamic (static) sharp-edge-of-chaos sub-domain of the coupling parameter plane of each cell, while in Fig. 12(b) ((c)) the choice of R and C sets one (both) cell(s) outside the sharp-edge-of chaos domain. The common pair (R, C) for each case in Fig. 12 is marked on the coupling parameter planes of the two cells in Figs. 11(a) and (b). It can be realized that steady-state oscillatory dynamics emerge in the network – see Fig. 12(a) – if and only if the common coupling parameter

Provided by Sächsische Landesbibliothek - Staats- und Universitätsbibliothek Dresden

Final edited form was published in "IEEE Transactions on Circuits and Systems : a publication of the IEEE Circuits and Systems Society. 1, Regular Papers. 2019, 66(7), S. 2627-2638. ISSN 1558-0806.
https://doi.org/10.1109/TCSI.2019.2894218

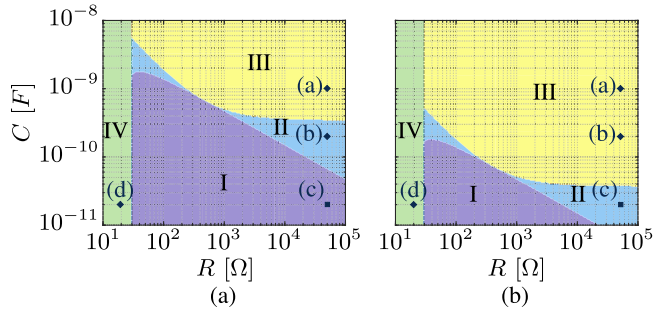

Fig. 11. RC parameter planes for the two cells with local input impedances $Z_1(s)$ (a) and $Z_2(s)$ (b), as in Figs. 9(a) and (b). Here, however, the locations of the common coupling parameter pairs relative to the subplots (a)-(d) of Fig. 12 are further highlighted.

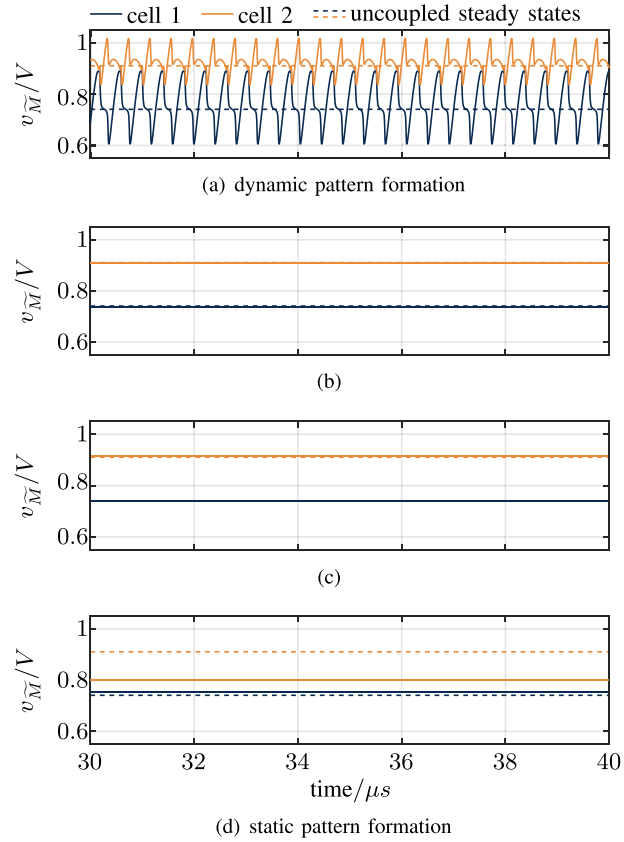

Fig. 12. Voltages dropping across the memristors of the two combined cells over time under different choices of the common coupling parameter pair. Cell 1 includes memristor $\widetilde{M}_1$, while cell 2 includes memristor $\widetilde{M}_2$. The uncoupled steady states are also depicted in each plot. (a) Coupling in the dynamic sharp-edge-of-chaos domain III for both cells; (b) Coupling in the edge-of-chaos domain II for cell 1 and in the dynamic sharp-edge-of-chaos domain III for cell 2; (c) Coupling in the locally passive domain for cell 1 and in the edge-of-chaos domain II for cell 2; (d) Coupling in the static sharp-edge-of-chaos domain IV for both cells.

combination is located in the dynamic sharp-edge-of-chaos domain III of the RC parameter plane for each cell. In such domain two zeros of the cell local input impedance form a complex conjugate pair with positive real part. In case the common choice of R and C sets each cell in the static sharp-edge-of-chaos domain IV, the cell in the network converges – see Fig. 12(d) – from the uncoupled steady state to a distinct steady state. If the common coupling parameter pair does not reside in the sharp-edge-of-chaos domain of the RC plane for each cell – see Fig. 12(b) and (c) – the emergence of asymptotic solutions different from the uncoupled steady states or of self-sustained oscillations cannot be observed, and the coupled cells are found to sit in the same stationary steady state of the uncoupled scenario. Thus, the coupling is waking the network up if and only if the common (R, C) pair lies in either of the sharp-edge-of-chaos sub-domains III and IV of the parameter plane for each cell. Connecting through a common coupling circuit several cells adopting memristors characterized by slightly different behaviors, caused, for example, by the intrinsic variability of their manufacturing process, the coupling parameter sub-space, where the network cells may support static or dynamic patterns, is obtained as the intersection between the sharp-edge-of-chaos domains in the parameter planes of the individual cells. Hence, reducing the variability in the electrical characteristics of the memristor devices becomes increasingly important for the future realization of large networks of coupled oscillators with locally-active memristors.

Clearly, the stationary (oscillatory) patterns, shown in Fig. 12(a) ((d)), originate from the operation of each network cell in the dynamic (static) sharp-edge-of-chaos domain III (IV), i.e. they are not merely the result of the interaction between two different nonlinear cells. In order to prove this claim, Fig. 13 depicts the voltage drops across the memristors of two identical combined cells, each characterized by the local input impedance $Z_1(s)$ (see Table II), for the four different coupling conditions highlighted in Fig. 11(a). As in the previous case, the simulations confirm the theoretical results. For the coupling parameter pair in the sharp-edge-of-chaos domain III (IV), dynamic (static) patterns form in the network at steady state, as illustrated in plot (a) (d) of Fig. 13. Unless both cells operate in a sharp-edge-of-chaos sub-domain, no static or dynamic pattern may ever emerge in the network, and each cell keeps in the common stationary steady state of the uncoupled scenario. Thus, the generation of patterns can be explained through the theory of local activity, and, particularly, of the edge-of-chaos.

B. Cell Array

Steady-state patterns can be also observed in larger M-CNNs. Let us present some numerical simulation results pertaining to a two-dimensional cellular array. Fig. 15 shows four temporally sequential snapshots of a dynamic pattern occurring in a 5×5 M-CNN. Here the 25 cells are assumed to be identical, each having memristor $\widetilde{M}_1$ (refer to Table I) and local input impedance $Z_1(s)$ (see Table II). The coupling parameters are chosen as $R = 1\,M\Omega$ and $C = 720\,pF$, and the cells are connected according to the von-Neumann arrangement, i.e. each cell is coupled only to its direct neighbors in the same row and column, as clear from Fig. 14. At the beginning of the simulation all voltages and currents in the network are set to zero. The voltage source V_S in each cell is ramped up to the DC value listed in Table II for cell 1, i.e. $9\,V$, within

Provided by Sächsische Landesbibliothek - Staats- und Universitätsbibliothek Dresden

Final edited form was published in "IEEE Transactions on Circuits and Systems : a publication of the IEEE Circuits and Systems Society. 1, Regular Papers. 2019, 66(7), S. 2627-2638. ISSN 1558-0806.
https://doi.org/10.1109/TCSI.2019.2894218

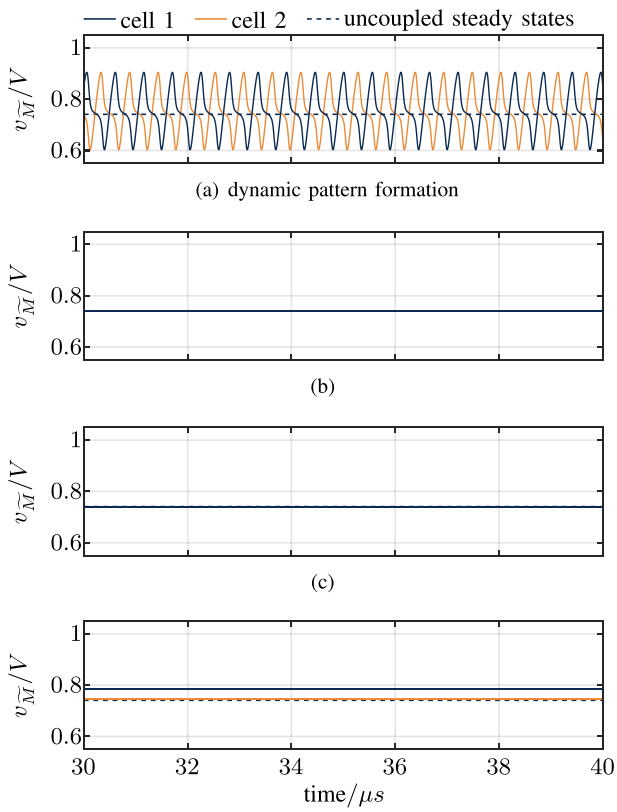

(a) dynamic pattern formation

(b)

(c)

(d) static pattern formation

Fig. 13. Voltages dropping across the memristors of two identical cells over time for 4 different choices of the common coupling parameter pair. Each cell contains the same memristor device, namely $\widetilde{M}_1$. The common uncoupled steady state is also depicted in each plot. (a) Coupling in the dynamic sharp-edge-of-chaos domain III for both cells; (b) Coupling in the edge-of-chaos domain II for both cells; (c) Coupling in the locally passive domain for both cells; (d) Coupling in the static sharp-edge-of-chaos domain IV for both cells.

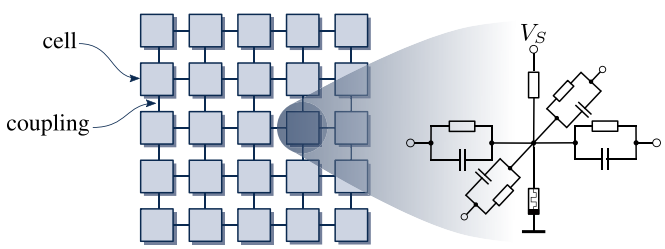

Fig. 14. Schematic diagram of the 5×5 M-CNN in von-Neumann arrangement.

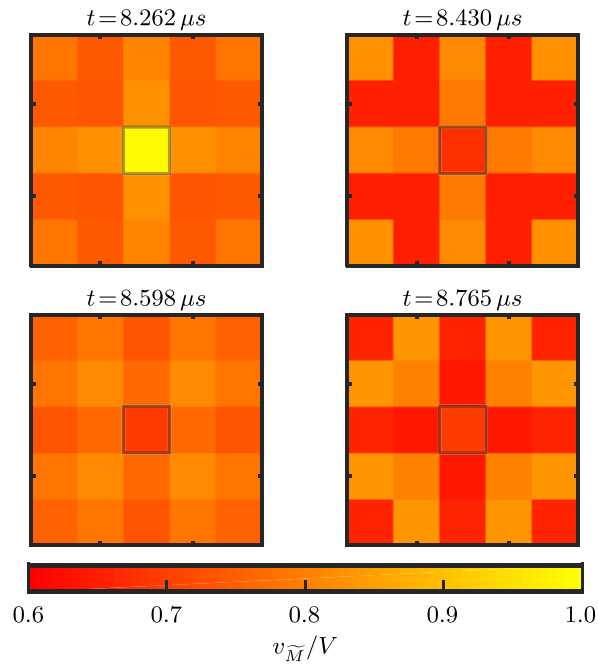

Fig. 15. Dynamic pattern formation in the 5×5 M-CNN of identical cells for a common coupling parameter pair in the dynamic sharp-edge-of-chaos domain III.

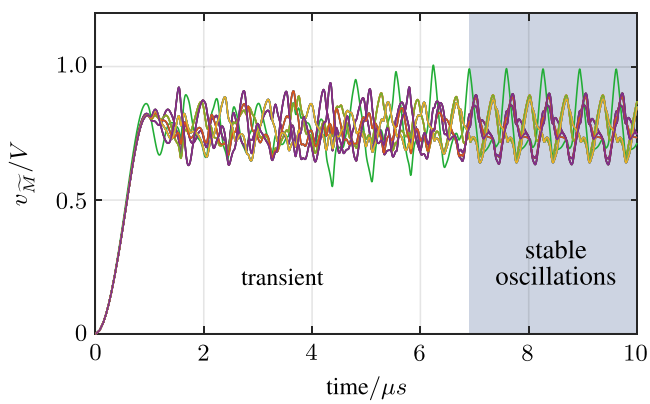

Fig. 16. Time evolution of the memristor voltages in all the 25 cells, as the network converges towards the dynamic pattern of Fig. 15.

the first microsecond. The ramp of the source voltage in the cell C(3,3) is commenced slightly before than for all the other cells. As shown in Fig. 16, stable oscillations emerge in the memristor cellular network after a transient phase. Particularly, the 4 snapshots, shown in Fig. 15, are recurring, giving origin to a complete cycle. For the formation of steady-state static patterns, the common coupling parameters have to be chosen in the static sharp-edge-of-chaos domain IV of the RC plane of cell 1. Here we choose the common coupling configuration marked as (d) in Fig. 11(a), which, in the network of two identical cells, led to the emergence of the steady-state static patterns depicted in Fig. 13(d). Two of the static patterns forming at steady state in the 5×5 memristor cellular array are presented in Fig. 17. Plot (a) shows a static pattern appearing in the M-CNN for the same initial condition scenario as in Fig. 15, where ramp of the source voltage in the center cell was slightly anticipated as compared to all the other cells. Fig. 17(b) shows the static pattern emerging in the network in case the ramp of the voltage source starts slightly earlier in cell C(2,2) than in the remaining M-CNN cells. Fig. 18 depicts the time evolution of the voltages falling across the memristors of all the cells as the network converges towards the static pattern shown in Fig. 17(a). Clearly, after a transient phase, the M-CNN reaches the steady state associated to the aforementioned static pattern. These simulations prove that tuning the initial conditions may modulate the steady-state static patterns forming asymptotically in the array of coupled memristor cells. Moreover, static patterns may also be

Provided by Sächsische Landesbibliothek - Staats- und Universitätsbibliothek Dresden

Final edited form was published in "IEEE Transactions on Circuits and Systems : a publication of the IEEE Circuits and Systems Society. 1, Regular Papers. 2019, 66(7), S. 2627-2638. ISSN 1558-0806.
https://doi.org/10.1109/TCSI.2019.2894218

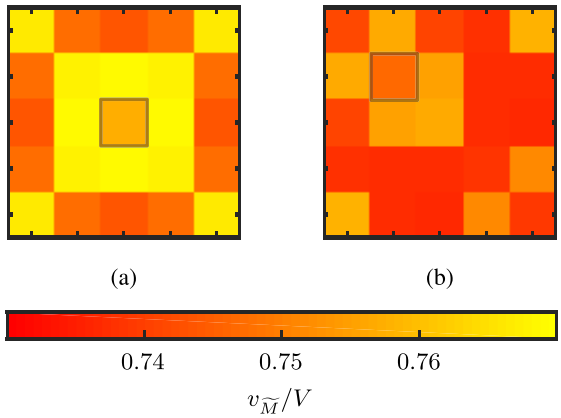

Fig. 17. Formation of a couple of distinct steady-state static patterns in the 5×5 M-CNN of identical cells for a common (R, C) pair located in the static sharp-edge-of-chaos domain IV. In (a) ((b)) the initialization of the cell C(3,3) (C(2,2)) is slightly out-of-phase as compared to all the other network cells.

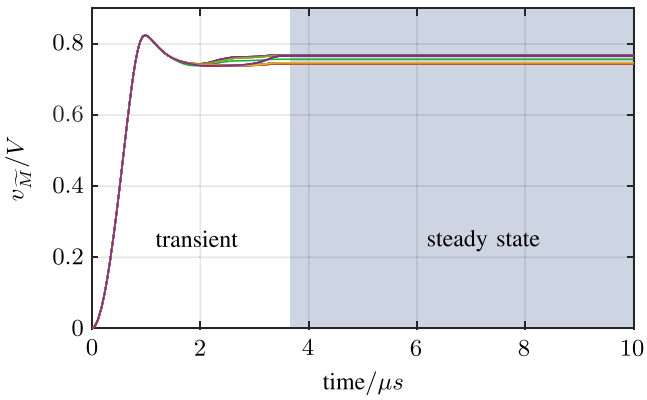

Fig. 18. Transient evolution of the memristor voltages in all the 25 M-CNN cells, as the network converges towards the static pattern shown in Fig. 17(a).

modified online by applying conditioning voltages to specific nodes in the network through suitable external sources.

VI. Conclusion

The analytical study presented in this paper is based on Chua's local activity theory and focuses on the investigation of the generation and control of complex behavior in a network of memristor cells depending upon the coupling conditions. Each of the cells in the nonlinear dynamic array consists of a NbO_x-based memristor and its DC biasing circuit. The cells are locally coupled through resistor-capacitor parallel one-ports. An in-depth analysis of the coupling parameters in the cellular network has unveiled the presence of two distinct sharp-edge-of-chaos regions in the locally-active and edge-of-chaos domain of the coupling parameter space. In the first region - domain III - the cell input impedance admits a pair of complex conjugate zeros with positive real part. Here the system support the emergence of dynamic patterns (see Fig. 15). The emergence of steady-state dynamic patterns in M-CNNs is of utmost importance for a future adoption of networks of this kind to implement novel signal processing strategies, e.g. a more efficient image encoding paradigm. In the second region - domain IV - the cell input impedance

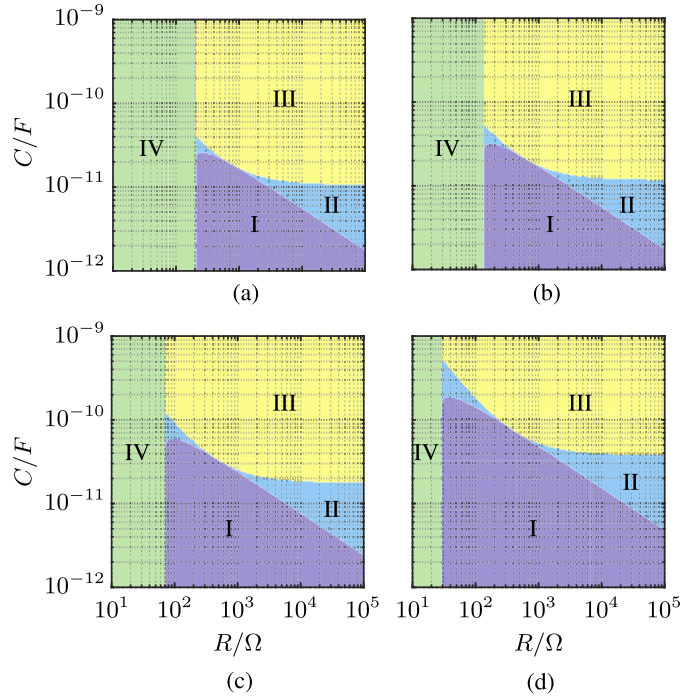

Fig. 19. RC parameter plane for cell 2 — employing memristor $\widetilde{M}_2$ and having local input impedance $Z_2(s)$ — for different operating points induced via changes in the DC-voltage source parameter V_S. The violet domain I contains parameter combinations where the cell is locally passive. The rest of the coupling parameter plane is the locally active domain, coinciding here with the edge-of-chaos domain. $Z_2(s)$ has no zeros with positive real part in the light blue domain II. No complex behavior emerges in the two-cell array if the (R, C) pair is located in such domain. The sharp-edge-of-chaos domain, where $Z_2(s)$ has a complex conjugate pair of zeros in the right half of the complex plane, is the yellow domain III, while the sharp-edge-of-chaos domain, where $Z_2(s)$ has one positive real zero, is the green domain IV. In domain III (IV) the network admits dynamic (static) patterns at the steady state.

admits a single zero with real and positive value. Here the system exhibit static patterns (see Figs. 17(a) and (b)). M-CNNs supporting the asymptotic formation of static patterns allow the implementation of other novel data processing methodologies, e.g. a faster image recognition technique based upon resonance effects. All in all, complex behavior emerge in the memristor network if and only if the coupling parameters are chosen for each cell either in region III or in region IV of the sharp-edge-of-chaos domain. Therefore the generation of steady-state spatial or temporal patterns can be induced in the network by means of a proper selection of the coupling parameters, and further modulated online through the application of conditioning voltages from external sources to specific nodes of the cellular array.

All our theoretical results were validated by measurements and numerical simulations of the memristive networks.

With regard to a future hardware implementation of large memristor arrays, such as those considered in the numerical study of section V-B, we have to take into account that non-ideal factors, most importantly the memristor device to memristor device variability, might degrade the overall system performance. Large arrays of cells in the sharp-edge-of-chaos might be unable to support the theoretically-predicted steady-state patterns under a considerable degree of device-to-device variability. Therefore, for the realization of large-scale

Provided by Sächsische Landesbibliothek - Staats- und Universitätsbibliothek Dresden

Final edited form was published in "IEEE Transactions on Circuits and Systems : a publication of the IEEE Circuits and Systems Society. 1, Regular Papers. 2019, 66(7), S. 2627-2638. ISSN 1558-0806.
https://doi.org/10.1109/TCSI.2019.2894218

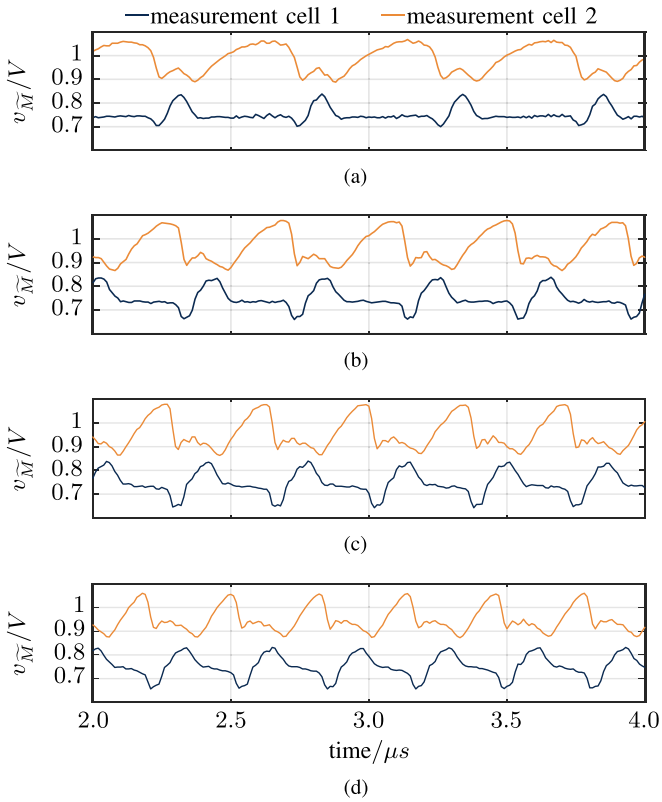

Fig. 20. Experimental measurements of the time waveforms of the voltages across the memristors of two distinct coupled cells. Each plot refers to a distinct value of the source voltage V_S in cell 2, whose operating point is thus subject to modifications, which affect the properties of the oscillations developing in the M-CNN.

memristor cellular networks, it is of fundamental importance to develop NbO_x nano-structures with more homogeneous dynamical behaviors. This is one of the research activities we are going to devote efforts upon in the near future. Another incoming research investigation shall target the derivation of optimal coupling parameter ranges, whereby all the network cells keep operating in the sharp-edge-of-chaos domain even under the non-negligible degree of variability, which currently characterizes the switching kinetics of distinct NbO_x memristor samples. Last but not least, the effects of device-to-device variability on the formation of patterns in M-CNN with alternative coupling circuits is also in our research activity agenda for the months to come.

All in all, based upon the promising results presented in this manuscript, networks of locally-coupled memristor cells in the sharp-edge-of-chaos are worthy of high consideration for the future implementation of novel data processing methodologies based upon the complex spatio-temporal phenomena which they are capable to support.

Appendix
Experimental Study of the Influence of the Cell Operating Point on the Development of M-CNN Oscillatory Solutions

In section IV we derived a map defining whether a pair of coupling parameters R and C chosen within prescribed variation intervals induce asymptotic pattern formation in the memristor cellular array. This map was determined for a specific operating point of each of the two cells. The operating points of the cells have a major impact on the steady-state dynamics of the network. In order to illustrate this point, Fig. 19 shows how the RC parameter plane of a cell with memristor $\widetilde{M}_2$ from Table I and local input impedance $Z_2(s)$ from Table II changes as the operating point is varied via the DC-voltage source parameter V_S. From Fig. 19 it can be easily inferred that the extension and shape of the various domains of the RC parameter plane change with the cell operating point. Particularly, the area of each of the sharp-edge-of-chaos domains III and IV shrinks as V_S is increased from $8\,V$ to $11\,V$. The cell operating point also plays a major role on the properties of the oscillatory solutions developing in a two-cell network when the common (R, C) parameter pair lies in the domain III. Fig. 20 illustrates the experimental oscillations developing across the memristors of two distinct cells — one employing memristor $\widetilde{M}_1$ from Table I and having local input impedance $Z_1(s)$ from Table II and the other employing memristor $\widetilde{M}_2$ from Table I and having local input impedance $Z_2(s)$ from Table II except for the value of source voltage V_S, which is taken here as control parameter — coupled through a RC bridge with $C = 720\,pF$ and $R = 1\,M\Omega$. Cell 2 remains in the dynamic sharp-edge-of-chaos domain in all the four scenarios illustrated in Fig. 20. However, as its source voltage parameter V_S is increased, the rise time of the steady-state voltage $v_{\widetilde{M}_2}$ falling across its memristor decreases, and, consequently, the frequency of the oscillations developing asymptotically in the M-CNN increases.

References

[1] D. B. Strukov, G. S. Snider, D. R. Stewart, and R. S. Williams, "The missing memristor found," *Nature*, vol. 453, no. 7191, p. 80, 2008.
[2] L. O. Chua, "Memristor-the missing circuit element," *IEEE Trans. Circuit Theory*, vol. CT-18, no. 5, pp. 507–519, Sep. 1971.
[3] L. Nicolosi, F. Abt, R. Tetzlaff, H. Hofler, A. Blug, and D. Carl, "New CNN based algorithms for the full penetration hole extraction in laser welding processes," in *Proc. IEEE Int. Symp. Circuits Syst.*, May 2009, pp. 2713–2716.
[4] M. D. Pickett, G. Medeiros-Ribeiro, and R. S. Williams, "A scalable neuristor built with mott memristors," *Nature Mater.*, vol. 12, no. 2, pp. 114–117, Dec. 2013.
[5] L. O. Chua, *CNN: A Paradigm for Complexity*, vol. 31. Cleveland, OH, USA: World Scientific, 1998.
[6] L. O. Chua, "Local activity is the origin of complexity," *Int. J. Bifurcation Chaos*, vol. 15, no. 11, pp. 3435–3456, 2005.
[7] A. Ascoli, S. Slesazeck, and H. Mähne, R. Tetzlaff, and T. Mikolajick, "Nonlinear dynamics of a locally-active memristor," *IEEE Trans. Circuits Syst. I, Reg. Papers*, vol. 62, no. 4, pp. 1165–1174, Apr. 2015.
[8] S. Datta, N. Shukla, M. Cotter, A. Parihar, and A. Raychowdhury, "Neuro inspired computing with coupled relaxation oscillators," in *Proc. 51st ACM/EDAC/IEEE Design Automat. Conf. (DAC)*, Jun. 2014, pp. 1–6.
[9] S. Li, X. Liu, S. K. Nandi, D. K. Venkatachalam, and R. G. Elliman, "Coupling dynamics of Nb/Nb_2O_5 relaxation oscillators," *Nanotechnology*, vol. 28, no. 12, p. 125201, Feb. 2017.
[10] A. A. Sharma, J. A. Bain, and J. A. Weldon, "Phase coupling and control of oxide-based oscillators for neuromorphic computing," *IEEE J. Explor. Solid-State Comput. Devices Circuits*, vol. 1, pp. 58–66, 2015, doi: 10.1109/JXCDC.2015.2448417.
[11] A. Ascoli, V. Lanza, F. Corinto, and R. Tetzlaff, "Synchronization conditions in simple memristor neural networks," *J. Franklin Inst.*, vol. 352, no. 8, pp. 3196–3220, Aug. 2015.

Provided by Sächsische Landesbibliothek - Staats- und Universitätsbibliothek Dresden

Final edited form was published in "IEEE Transactions on Circuits and Systems : a publication of the IEEE Circuits and Systems Society. 1, Regular Papers. 2019, 66(7), S. 2627-2638. ISSN 1558-0806.
https://doi.org/10.1109/TCSI.2019.2894218

[12] G. A. Gibson *et al.*, "An accurate locally active memristor model for s-type negative differential resistance in NbO_x," *Appl. Phys. Lett.*, vol. 108, no. 2, p. 023505, 2016.
[13] C. Funck *et al.*, "Multidimensional simulation of threshold switching in NbO_2 based on an electric field triggered thermal runaway model," *Adv. Electron. Mater.*, vol. 2, no. 7, p. 1600169, Jul. 2016.
[14] A. S. Alexandrov, A. M. Bratkovsky, B. Bridle, S. Savel'ev, D. B. Strukov, and S. R. Williams, "Current-controlled negative differential resistance due to Joule heating in TiO_2," *Appl. Phys. Lett.*, vol. 99, no. 20, p. 202104, Nov. 2011.
[15] R. S. Williams, M. D. Pickett, and J. P. Strachan, "Physics-based memristor models," in *Proc. IEEE Int. Symp. Circuits Syst.*, May 2013, pp. 217–220.
[16] S. Slesazeck *et al.*, "Physical model of threshold switching in NbO_2 based memristors," *RSC Adv.*, vol. 5, no. 124, pp. 102318–102322, 2015.
[17] S. Slesazeck, M. Herzig, T. Mikolajick, A. Ascoli, M. Weiher, and R. Tetzlaff, "Analysis of V_{th} variability in NbO_x-based threshold switches," in *Proc. 16th Non-Volatile Memory Technol. Symp. (NVMTS)*, Oct. 2016, pp. 1–5.
[18] R. G. Breckenridge and W. R. Hosler, "Electrical properties of titanium dioxide semiconductors," *Phys. Rev. J. Arch.*, vol. 91, no. 4, p. 793, Aug. 1953.
[19] J. Honig and T. Reed, "Electrical properties of Ti_2O_3single crystals," *Phys. Rev.*, vol. 174, no. 3, p. 1020, 1968.
[20] J. Radhakrishnan, S. Slesazeck, H. Wylezich, T. Mikolajick, A. Ascoli, and R. Tetzlaff, "A physics-based Spice model for the Nb_2O_5 threshold switching memristor," in *Proc. 15th Int. Workshop Cellular Nanosc. Netw. Appl.*, Aug. 2016, pp. 1–2.
[21] S. K. Nandi, X. Liu, D. K. Venkatachalam, and R. G. Elliman, "Threshold current reduction for the metal-insulator transition in NbO_{2-x}-selector devices: The effect of ReRAM integration," *J. Phys. D, Appl. Phys.*, vol. 48, no. 19, p. 195105, Apr. 2015.
[22] X. Liu, S. Li, S. K. Nandi, D. K. Venkatachalam, and R. G. Elliman, "Threshold switching and electrical self-oscillation in niobium oxide films," *J. Appl. Phys.*, vol. 120, no. 12, p. 124102, Sep. 2016.
[23] L. O. Chua, "Memristor, hodgkin–huxley, and edge of chaos," *Nanotechnology*, vol. 24, no. 38, p. 383001, Sep. 2013.
[24] S. Slesazeck, A. Ascoli, and H. Mähne, R. Tetzlaff, and T. Mikolajick, "Unfolding the threshold switching behavior of a memristor," in *Proc. Int. Conf. Nonlinear Dyn. Electron. Syst.* Albena, Bulgaria: Springer, 2014, pp. 156–164.
[25] P. O. Vontobel, W. Robinett, P. J. Kuekes, D. R. Stewart, J. Straznicky, and R. S. Williams, "Writing to and reading from a nano-scale crossbar memory based on memristors," *Nanotechnology*, vol. 20, no. 42, p. 425204, 2009.
[26] B. Yan, C. Liu, X. Liu, Y. Chen, and H. Li, "Understanding the tradeoffs of device, circuit and application in reram-based neuromorphic computing systems," in *IEDM Tech. Dig.*, Dec. 2017, pp. 4–11.

Martin Weiher received the Diploma degree in electrical engineering, with the specialization in control theory, from the Technische Universität Dresden, Dresden, Germany. He is currently a Research Associate with the Chair of Fundamentals of Electrical Engineering, Technische Universität Dresden. His research interests include nonlinear systems, model identifications especially for memristive systems, and networks of coupled memristive cells and their applications in signal processing.

Melanie Herzig received the B.S. degree in applied science and the M.S. degree in photovoltaic and semiconductor technology from the Technische Universität Freiberg, Freiberg, Germany, in 2012 and 2015, respectively. She is currently pursuing the Ph.D. degree in electrical engineering with NaMLab gGmbH, Dresden, Germany. Her research interests include fabrication and optimization of as well as nonlinear circuits based on memristive devices.

Ronald Tetzlaff is currently a Full Professor of fundamentals of electrical engineering with the Technische Universität Dresden, Dresden, Germany. His scientific interests include problems in the theory of signals and systems, medical signal processing, stochastic processes, system modeling, system identification, machine learning, mem-elements, memristive systems, Volterra systems, and cellular nonlinear networks.

Alon Ascoli received the Ph.D. degree in electronic engineering from University College Dublin in 2006. Since 2012, he has been with the Faculty of Electrical and Computer Engineering, Technische Universität Dresden, where he is currently pursuing the Habilitation in the scientific area of fundamentals of electrical engineering. Since 2018, he has been a Scientific Collaborator with the Department of Microelectronics, Brno University of Technology, Brno, Czech Republic. His research interests lie in the area of nonlinear circuits and systems, networks of oscillators, cellular nonlinear networks, and memristors. He was honored with the IJCTA 2007 Best Paper Award. In 2017, he was conferred the habilitation title as an Associate Professor in electrical circuit theory from the Italian Ministry of Education.

Thomas Mikolajick received the Diploma degree in electrical engineering, and the Ph.D. degree in electrical engineering from University Erlangen-Nuremberg, Germany, in 1990 and 1996, respectively. In 2009, he was with the Technische Universität Dresden, Dresden, Germany, where he is currently holding a professorship for nano-electronic materials, in combination with the position of Scientific Director with NaMLab gGmbH. His research focuses on emerging non-volatile memories.

Stefan Slesazeck received the Ph.D. degree in microelectronics from the Technische Universität Dresden, Dresden, Germany, in 2004. He joined Qimonda Dresden as a Device Engineer, and has focused on the pre-development of the 3D DRAM access devices and concept evaluation for 1T – DRAM. In 2009, he joined NaMLab gGmbH. As a Senior Scientist, he is responsible for the device and concept development, electrical characterization, and modeling of memories.

Provided by Sächsische Landesbibliothek - Staats- und Universitätsbibliothek Dresden